Post-print version of the paper by Grimsmo et al. in J Constr Steel Res, 126 (2016) 15-25
http://dx.doi.org/10.1016/j.jcsr.2016.06.023

Failure modes of bolt and nut assemblies under tensile loading

E. L. Grimsmo*, A. Aalberg, M. Langseth, A. H. Clausen

Structural Impact Laboratory (SIMLab) and Centre for Advanced Structural Analysis (CASA), Department of Structural Engineering, Norwegian University of Science and Technology, NO-7491 Trondheim, Norway
*Corresponding author. Email address: erik.l.grimsmo@ntnu.no.

Abstract

Thread failure of bolt and nut assemblies subjected to tension is generally undesired because it is a less ductile failure mode than fracture of the threaded shank of the bolt (denoted bolt fracture). Another issue is that incipient failure of the threads due to over-tightening is difficult to detect during installation. Thus, it is appropriate to investigate the causes of thread failure. A parameter that seems to govern the failure mode of bolt and nut assemblies, despite receiving limited attention in the literature, is the length L_t of the threaded bolt shank located within the grip. This is particularly relevant for partially threaded bolts, where L_t may be short. In the current study, direct tension tests were performed on M16 bolt and nut assemblies with different lengths L_t. The tests showed that $L_t \leq 9$ mm resulted in thread failure, whereas $L_t \geq 17$ mm resulted in bolt fracture. For the intermediate range of L_t, both failure modes were observed in replicate tests. Validated finite element simulations were conducted to gain insights into the mechanisms of failure. When L_t was short, necking of the bolt occurred close to the nut so that the overlap between the threads of the bolt and the nut was reduced, which further induced thread failure. This paper suggests several practical approaches for reducing the probability of thread failure.

Keywords: bolts; failure; tension; experiments; simulations

1 Introduction

There are three common failure modes of bolt and nut assemblies under tension: bolt fracture, bolt thread failure, and nut thread failure. Hereafter, the two latter failure modes are both denoted as thread failure. This paper demonstrates that using partially rather than fully threaded bolts in

connections may increase the chance of thread failure. This failure mode is less ductile than bolt fracture and is therefore generally not desired. Another important aspect noted by Alexander [1] is that incipient thread failure may go undetected when over-tightening bolt assemblies during installation of a structure because it is a gradual failure process. Thus, the assembled structure may enter service with weakened or partially failed fasteners.

The standard ISO 898-2: *Mechanical properties of fasteners made of carbon steel and alloy steel – Part 2* [2] states that bolt fracture is the intended fracture mode of bolt and nut assemblies with regular nuts. Additionally, other references emphasize that threaded fasteners loaded under tension should fail by bolt fracture and not by thread failure [3, 4]. Despite this, thread failure in destructive tests of bolted connections seems to be a recurring phenomenon [5-9]. Moreover, Grimsmo et al. [10] performed tests on bolted end-plate connections of the type shown in Figure 1a, where the intended failure mode was end-plate bending deformation combined with tensile bolt fracture. The moment vs. rotation of the joint curves displayed in Figure 1b were determined from two replicate quasi-static tests, where one nut per bolt was used in one test and two nuts in the other. Employing one nut led to thread failure, whereas two nuts led to bolt fracture. Furthermore, two nuts gave an approximately 10% increase in the maximum measured joint moment and a 130% increase of the joint rotation upon initiation of bolt failure. In this case, it is clear that bolt fracture would be preferred. Note that end-plate connections are conventionally designed so that the connections fail by end-plate bending only, and not by bolt fracture.

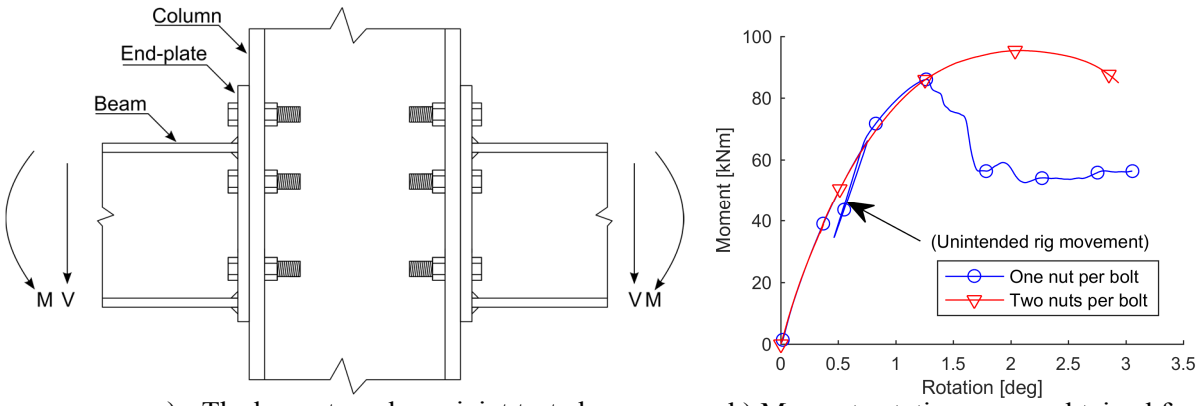

a) The beam-to-column joint tested

b) Moment-rotation curves obtained from two tests on the joint type shown in a)

Figure 1 - Grimsmo et al. [10] tested beam-to-column joints with one and two nuts per bolt.

Post-print version of the paper by Grimsmo et al. in J Constr Steel Res, 126 (2016) 15-25
http://dx.doi.org/10.1016/j.jcsr.2016.06.023

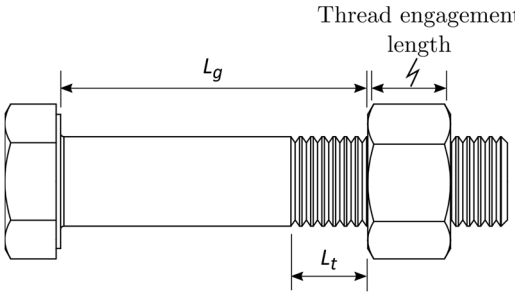

Figure 2 - Definitions of grip length L_g, threaded length L_t, and thread engagement length.

The failure mode of bolt and nut assemblies subjected to tensile loading is determined by several factors, such as geometry and dimensions (e.g., the cross-sectional area of the bolt, thread dimensions, and thread engagement length), mechanical properties of the bolt and nut material, and the length L_t the of bolt shank located within the grip length L_g. These lengths are defined in Figure 2 along with the thread engagement length, which is slightly shorter than the nut height due to countersinks on both sides of the nut.

The primary objective of this paper is to study how the threaded length L_t affects the tensile behaviour of bolt and nut assemblies, particularly in terms of the failure mode. There are few studies on this topic in the literature. Troup and Chesson [11], and Sterling and Fisher [12] performed both direct and torqued tension tests on ASTM A490 bolt and nut assemblies. They observed more occurrences of thread failure in bolt assemblies when L_t was reduced, but they gave no substantial explanation for this result. Alexander [1] briefly discussed how few threads within the grip, i.e., short threaded length L_t, may induce thread stripping due to necking of the bolt occurring close to the engaged threads. Unfortunately, he did not provide results from experimental studies. More recently, Fransplass et al. [13, 14] studied the behaviour of threaded rods at elevated strain rates. They observed that reducing the number of threads within the grip length changed the failure mode from shank failure to thread failure, both in tests and in numerical simulations. The rods were screwed into threaded holes in bars with much higher strength, which experienced practically no deformation during the tests. Thus, the work by Fransplass et al. did not incorporate the effects from internal thread deformation and nut dilatation, i.e., outward radial displacement of the nut.

Note that the available literature is ambiguous in terms of the influence of the threaded length L_t on the failure mode. Amrine and Swanson [15] experienced only bolt fracture when they tested

ASTM A325 bolt and nut assemblies with a varying number of threads in the grip. Nevertheless, to our knowledge, no publications in the literature have the purpose of investigating how the threaded length L_t affects the failure mode in bolt and nut assemblies.

The current paper presents results from a series of direct tension tests on partially and fully threaded bolt and nut assemblies, where the grip length L_g, and thus the threaded length L_t, was varied. A finite element (FE) model of the tests is also presented, primarily for investigating the mechanisms determining the failure modes and for evaluating the test results. After validating the FE model against the experimental tests, the model was employed to investigate how the response was affected by varying the yield strength and hardening of the nut, and whether thread failure could be prevented by using a high nut.

This article is organised as follows. Section 2 specifies the types of bolt and nuts used in the experimental programme. The results from the material tests obtained from standard uniaxial tension tests and hardness measurements are provided in Section 3. In Section 4, the setup and results of the tests on the bolt and nut assemblies are presented. The FE model and simulation results follow in Section 5. Finally, discussions and conclusions are provided in Sections 6 and 7, respectively.

2 Bolt and nut specimens

The tested bolts were partially threaded (PT) or fully threaded (FT) M16 × 160 mm bolts of grade 8.8 manufactured according to the standards ISO 4014: *Hexagon head bolts* [16] and ISO 4017: *Hexagon head screws* [17], respectively. The property class of the nuts was 8, and they were manufactured according to ISO 4032: *Hexagon regular nuts* [18]. Figure 3 shows the two types of bolt and nut assemblies tested herein. The chosen specimens were generic bolts and nuts, in that they were not certified according to the standards NS-EN 15048-1: *Non-preloaded structural bolting assemblies – Part 1* [19] or NS-EN 14399-1: *High-strength structural bolting assemblies for preloading - Part 1* [20]. Nevertheless, the results in Section 4.2 demonstrate that the bolt and nut assemblies satisfied the minimum tensile resistance requirement (130 kN) of the former standard. Moreover, the bolts and nuts are shown to satisfy the relevant requirements of mechanical properties and dimensions found in appropriate ISO standards.

Post-print version of the paper by Grimsmo et al. in J Constr Steel Res, 126 (2016) 15-25
http://dx.doi.org/10.1016/j.jcsr.2016.06.023

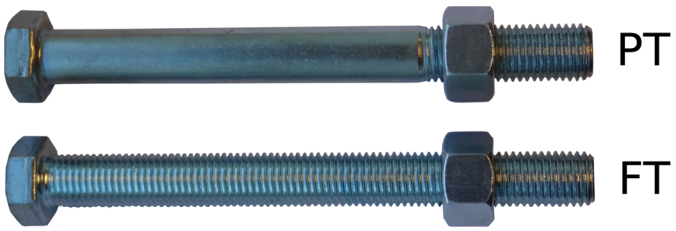

Figure 3 - Photo of the two types of bolt and nut assemblies employed in the tests, one with a partially threaded (PT) bolt and the other with a fully threaded (FT) bolt. The grip length $L_g = 118$ mm for both these assemblies.

3 Material tests

3.1 Tension tests

Quasi-static tension tests were performed on specimens machined from both the partially (PT) and fully threaded (FT) bolts. As depicted in Figure 4, the uniaxial tension specimens were machined to a reduced diameter of 12 mm over a parallel length of 72 mm. The tests were conducted in a screw-driven machine at a strain rate on the order of 10^{-4} s^{-1}. All the tests were monitored with a digital camera. A speckle pattern was sprayed on the specimens so that local strains in the neck could be acquired from digital image correlation (DIC) analyses.

Five replicate material tests were performed on each of the two bolt types, PT and FT, giving the results shown in Figure 5. The engineering strain was determined by DIC analysis. As observed in the figure, the PT bolt material is clearly stronger, both in terms of yield and ultimate strength. Average ultimate strengths of 963.5 and 922.1 MPa were found for the PT and FT bolt materials, respectively. Another feature that separated the two materials was that only the PT bolt material provided a distinct yield plateau; see Figure 5. The average stress value of the yield plateau for the PT bolts was 908.7 MPa, whereas the average stress value at the first indication of yield for the FT

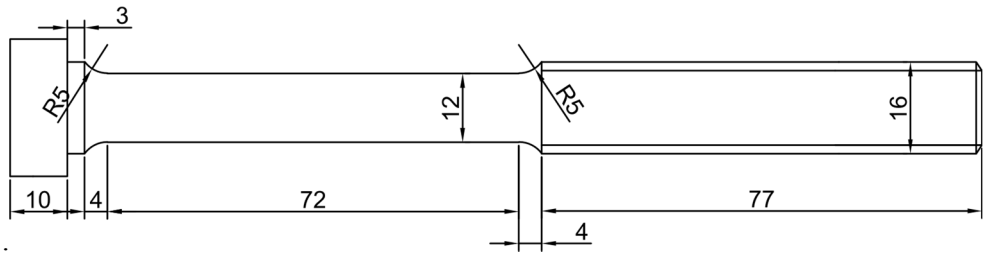

Figure 4 - Dimensions of test specimens employed in uniaxial tension tests (material tests).

bolts was 796.5 MPa. Section 5.2 provides material model parameters identified from the material tests.

3.2 Hardness tests

The hardness variation over cross-sections of the bolts and nuts was determined by conducting standard Vickers hardness tests, where a 10 kgf load was applied for 10 seconds. The Vickers numbers (HV) obtained from the hardness tests on a nut cross-section are provided in Figure 6. No distinct variations of hardness were found, and the average hardness was 231 HV with a standard deviation (SD) of 7 HV. Similarly, measurements carried out on PT and FT bolts did not reveal any clear variation of hardness over cross-sections of the bolts. Fifteen indentations were performed on each of the bolt cross-sections, and the average hardness values were 301 HV (SD: 3 HV) and 293 HV (SD: 7 HV) for the PT and FT bolts, respectively. It is reasonable that the PT bolts had a slightly higher hardness than the FT bolts when considering the material test results, which showed that the PT bolts were stronger; see Figure 5. The hardness measurements meet the requirements in the standards ISO 898-1 [21] and ISO 898-2 [2], which state that the HV values should be in the range of 255-335 for the bolts and 200-302 for the nuts.

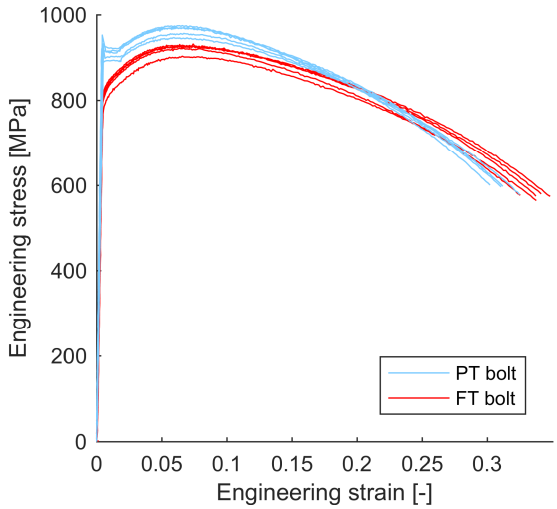

Figure 5 - Engineering stress-strain curves obtained from the uniaxial tension tests (material tests).

Post-print version of the paper by Grimsmo et al. in J Constr Steel Res, 126 (2016) 15-25
http://dx.doi.org/10.1016/j.jcsr.2016.06.023

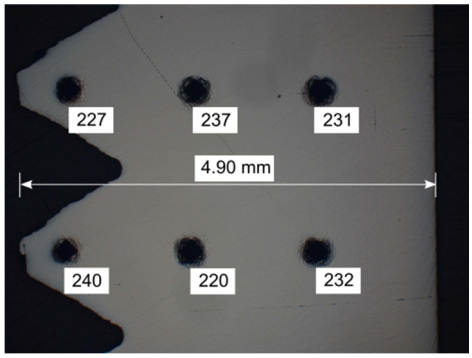

Figure 6 - Results from Vickers hardness tests on a nut cross-section. The dark dots show where the indenter was inserted.

The hardness of the nuts was clearly lower than of the bolts. This was expected because there are differences in the manufacturing processes of these two components, e.g., the threads of the bolts are made by roll threading, whereas the nuts are tapped. The hardness of a material is commonly assumed proportional to its yield strength. Thus, the yield stress of the nut can be estimated from the differences in hardness by

$$\sigma_{y,nut} = (HV_{nut}/\mathrm{HV}_{bolt})\sigma_{y,bolt} = (231/301) \cdot 908.7 \text{ MPa} = 697.4 \text{ MPa}$$

The accuracy of this estimation is investigated by FE simulations in Section 5.5.

4 Component tests

4.1 Test setup and programme

The tests on the bolt and nut assemblies depicted in Figure 3 were carried out in an Instron screw-driven testing machine equipped with two identical grips designed for testing of such assemblies. Figure 7a shows how the bolt assemblies were mounted. Two 25 mm thick circular steel plates with 18 mm diameter holes were placed within the grips such that the test specimens experienced tension as the grips moved apart. A ball-and-socket type of joint in the grips ensured that no bending moments were transferred to the bolt assembly. The tests were conducted by fixing the lower grip and applying a constant displacement rate to the upper grip. Figure 7b provides additional details on the test setup. Note that 25 mm long steel bushings were inserted into the bolt holes, which ensured that the bolt was located concentrically with the holes. These bushings were required to obtain good reproducibility in the replicate tests.

Post-print version of the paper by Grimsmo et al. in J Constr Steel Res, 126 (2016) 15-25
http://dx.doi.org/10.1016/j.jcsr.2016.06.023

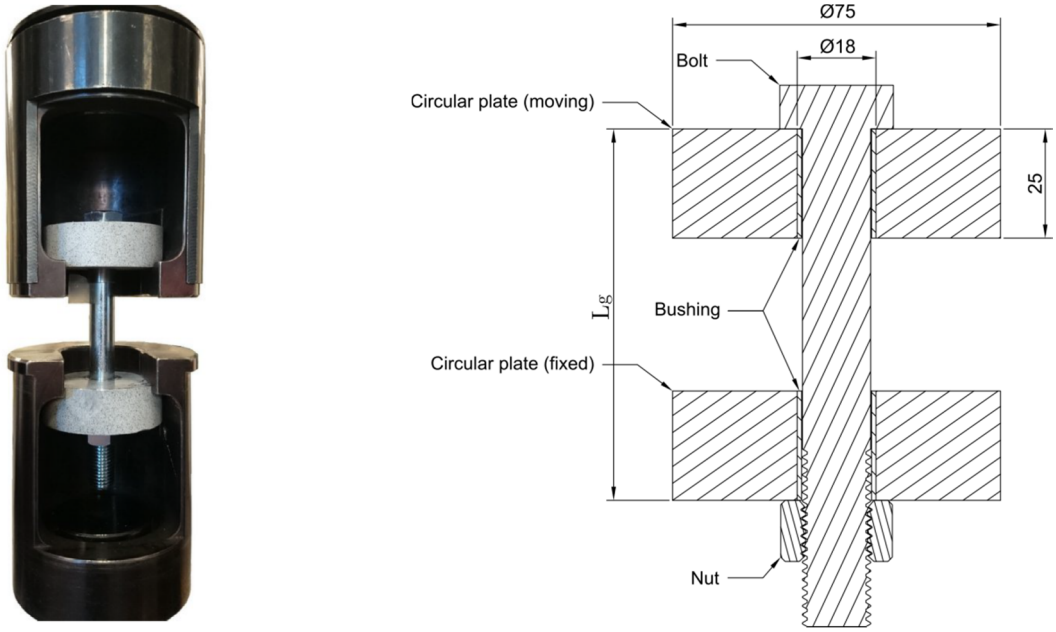

a) Photo of a bolt mounted in the purpose-made grips

b) Cross-section view of a test specimen and the circular plates

Figure 7 - The test setup for tension tests of bolt and nut assemblies.

Table 1 presents a survey of the experimental programme and several key results. As indicated in the first two columns of the table, tests were conducted for seven grip lengths L_g for the PT bolt assemblies and two for the FT bolt assemblies. The chosen grip lengths L_g ranged from 118 to 141 mm for both bolt types. Five replicate tests were performed for each of the nine configurations.

Table 1 also provides the corresponding threaded length L_t (column 3) and the number of full threads within the grip length (column 4). Due to the smaller cross-sectional area at the threaded length compared with the unthreaded length of the bolts, all the plastic deformation occurred within the threaded length. Therefore, the applied displacement rate was selected as 0.8 mm/min for the PT bolts and 2.0 mm/min for the FT bolts because the FT bolts had a significantly longer threaded length L_t over which plastic deformation occurred.

Post-print version of the paper by Grimsmo et al. in J Constr Steel Res, 126 (2016) 15-25
http://dx.doi.org/10.1016/j.jcsr.2016.06.023

Table 1 - Summary of the test programme and results. The force and displacement values represent the averages obtained from five replicate tests. Abbreviations: PT = partially threaded and FT = fully threaded.

Bolt type	Grip length L_g [mm]	Threaded length L_t [mm]	No. of threads in grip length	Avg. max. force [kN]	Avg. failure displ. [mm]	No. of thread failures	No. of bolt fractures
PT	118	5	2	151.8	4.3	5	0
PT	122	9	4	152.4	4.8	5	0
PT	124	11	5	151.0	5.2	4	1
PT	126	13	6	149.1	6.0	3	2
PT	128	15	7	149.2	6.9	2	3
PT	130	17	8	149.1	8.6	0	5
PT	141	28	13	147.3	9.5	0	5
FT	118	115	57	140.8	16.3	0	5
FT	141	138	69	140.9	18.2	0	5

The test machine provided the cross-head displacement, and a load cell mounted in the machine measured the force applied to the test specimen. Two of the five replicate tests for each grip length were monitored with a digital camera during the entire test. Local displacement measurements were facilitated by applying a speckle-pattern to the head of the bolt and the nut so that the displacement of the head of the bolt with respect to the nut could be accurately determined through digital image correlation (DIC) analysis.

4.2 Results

Figure 8 shows the force-displacement curves obtained from partially threaded (PT) and fully threaded (FT) bolts with an identical grip length $L_g = 118$ mm, which is the configuration depicted in Figure 3. The replicate tests displayed good repeatability, both in terms of the force-displacement curves and the displacement at failure. The average maximum force of the five replicate tests is given in column 5 of Table 1. Figure 8 and Table 1 show that a greater maximum force (approx. 8%) was obtained for the PT bolts. This was partly caused by the higher strength of the PT bolts noted in Section 3.1. An additional increase in force for the PT bolts occurred because necking of the bolt had to take place within the relatively short threaded length L_t. The unthreaded shank restricts formation of the neck, and this effect is analogous to tension tests on notched specimens, where the notch induces a triaxial state of stress allowing for enhanced stress levels. The consequence of this effect is observed from the average maximum force of the PT bolts in Table 1, where the force is generally higher for shorter threaded lengths.

Post-print version of the paper by Grimsmo et al. in J Constr Steel Res, 126 (2016) 15-25
http://dx.doi.org/10.1016/j.jcsr.2016.06.023

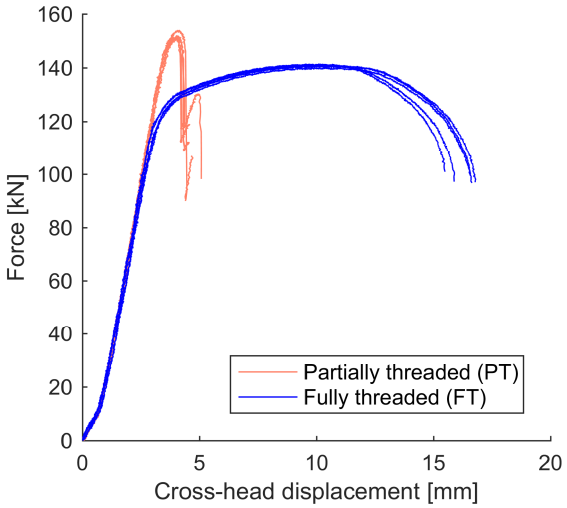

Figure 8 - Force-displacement curves obtained from five replicate tests performed on PT and FT bolts with an identical grip length $L_g = 118$ mm (corresponding to threaded lengths of 5 and 115 mm for the PT and FT bolts, respectively).

Column 6 of Table 1 provides the average cross-head displacement at failure of the five replicate tests. Here, failure is defined as the instant there was a sudden reduction in force. As observed from the table and Figure 8, the FT bolts experienced a significantly larger displacement before failure than the PT bolts. This is mainly due to the longer threaded length L_t available within the grip for the FT bolts. The last two columns of Table 1 indicate that all five PT bolts with grip length $L_g = 118$ mm (corresponding to $L_t = 5$ mm) failed prematurely by thread failure, whereas the five FT bolts with the same grip length (corresponding to $L_t = 115$ mm) failed by bolt fracture following significant diffuse necking. This difference in failure mode contributed to an even larger discrepancy in the displacement at failure for the two bolt types.

All the fully threaded (FT) bolts experienced bolt fracture. In contrast, the partially threaded (PT) bolts changed failure mode from thread failure to bolt fracture as the grip length L_g, and hence the threaded length L_t, increased. As indicated in Table 1, for $L_t \leq 9$ mm, thread failure was exclusively obtained. Both types of failure modes occurred for $11 \leq L_t \leq 15$ mm, and the probability of thread failure seemed to decrease with increasing threaded length; see the last two columns of Table 1. For $L_t \geq 17$ mm, only bolt fracture was observed.

Force-displacement curves for PT bolts with threaded lengths L_t of 9, 11, 15, and 17 mm are provided in Figure 9. Similar to the curves in Figure 8, thread failure caused the force to suddenly

drop before any gradual reduction developed. Considering Figure 9b and c, thread failure clearly led to a reduction in the displacement at failure, or ductility, whereas the obtained maximum force was practically the same for the two failure modes of bolt fracture and thread failure.

At maximum force, diffuse necking of the threaded bolt shank initiated, which seems to have induced thread failure in some of the tests. Indeed, the FE simulations in Section 5.4 demonstrate how the necking process influenced the failure mode. For the tests that did not fail at incipient necking, formation of the neck continued and the force gradually decreased. This consequently reduced the loading on the engaged threads and prevented the occurrence of thread failure at a later stage. These tests eventually failed by bolt fracture. The slightly greater force observed for the shorter threaded lengths (see Table 1) implies that the engaged threads experienced a corresponding greater load. In addition to neck formation, this effect may have contributed to thread failure, as suggested by Troup and Chesson [11].

As mentioned, both failure modes were observed in tests with threaded lengths of $11 \leq L_t \leq 15$ mm. In this range, the failure mode was governed by the threaded length, as well as other factors, such as small variations in the material strength, which is seen in Section 3.1. Strength variation may also explain the noticeable scatter in the displacement at failure in the tests that experienced thread failure; see particularly Figure 9a and b.

Post-print version of the paper by Grimsmo et al. in J Constr Steel Res, 126 (2016) 15-25
http://dx.doi.org/10.1016/j.jcsr.2016.06.023

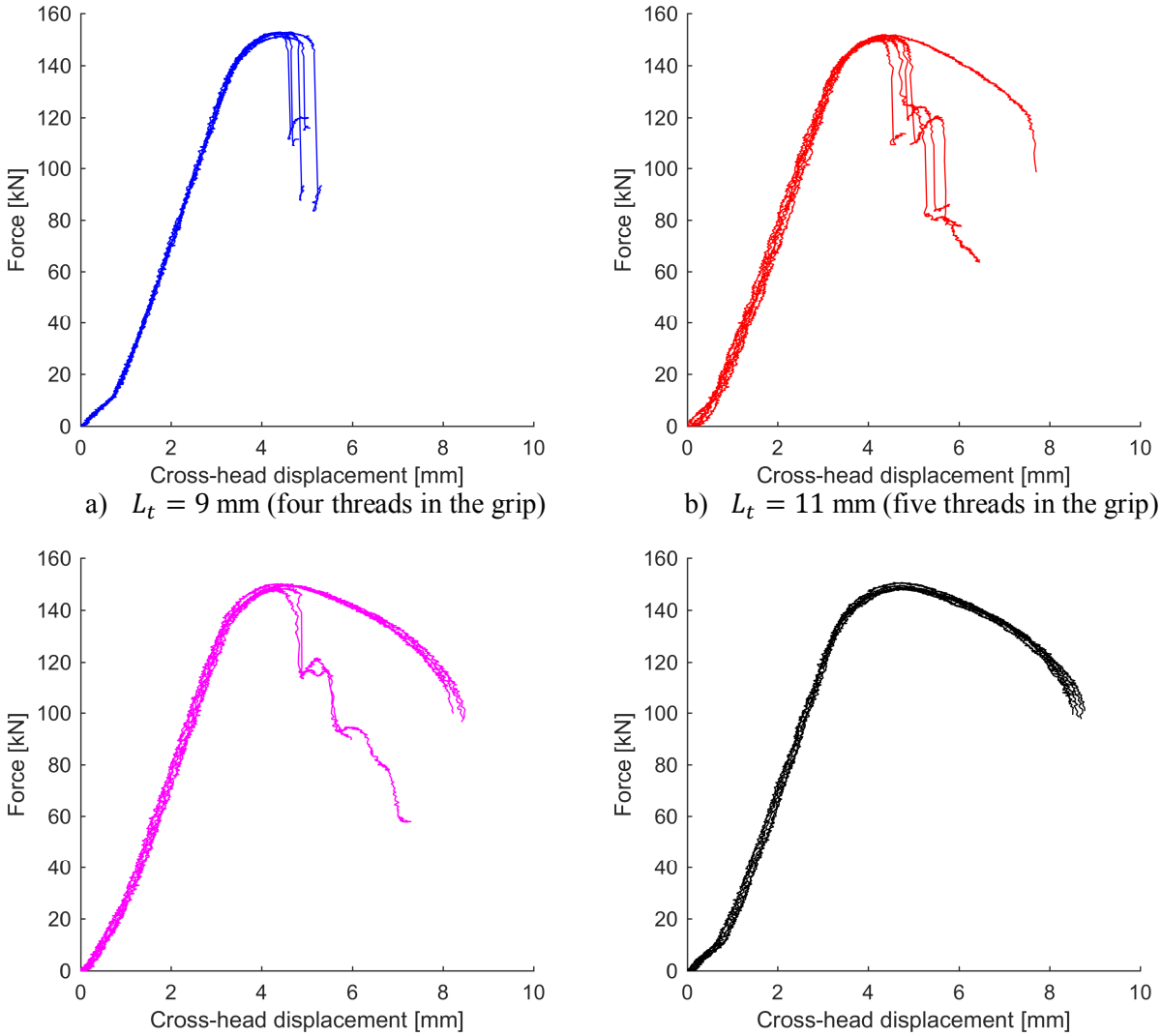

a) $L_t = 9$ mm (four threads in the grip)
b) $L_t = 11$ mm (five threads in the grip)
c) $L_t = 15$ mm (seven threads in the grip)
d) $L_t = 17$ mm (eight threads in the grip)

Figure 9 - Force-displacement curves obtained from partially threaded bolts with different threaded lengths.

Figure 10a shows how the threads of a PT bolt failed when tested with a threaded length $L_t = 9$ mm, i.e., four threads within the grip. Note that five of the bolt threads were properly engaged with the nut. As displayed in the figure, the uppermost engaged thread of the bolt was stripped or sheared off. The three threads below that thread were mostly bent, whereas the bottommost engaged thread was also sheared off. As observed from the FE simulations in Section 5.4, these threads failed differently due to the shape of the threads of the nut. Figure 10b shows a specimen that failed by bolt fracture for $L_t = 11$ mm. Most of the bolts that failed by bolt fracture obtained a slanted type of fracture surface like the one in Figure 10b. The others attained a more cup-and-cone type of fracture surface.

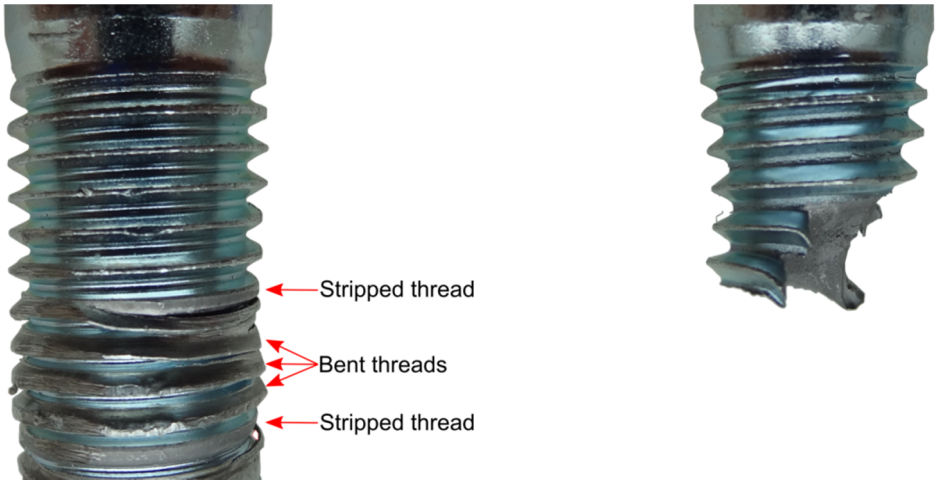

a) Thread failure (PT bolt, $L_t = 9$ mm) b) Bolt fracture (PT bolt, $L_t = 11$ mm)

Figure 10 - Photos of the two experienced failure modes.

5 Finite element simulations

Finite element (FE) simulations were conducted using the commercial software Abaqus/Explicit v6.14 [22]. The explicit solver was employed because it allows for element erosion. The presentation herein is limited to the simulations of the tests with partially threaded (PT) bolts because only these specimens displayed a change in failure mode when the threaded length L_t was varied.

5.1 Geometry and mesh

Tiny elements with dimensions on the order of 0.1 mm are necessary at the threads for enabling a proper simulation of possible thread failure. Such small elements lead to a very small stable time increment in the explicit analyses and thus a large computational cost. An axisymmetric model was employed to limit the required computational effort because a three-dimensional model with the same mesh density would be impractical for the purposes of this study.

The actual dimensions of the threads were determined by taking high-resolution photos of the cross-sections of bolts and nuts, as shown in Figure 11. By determining the pixel-to-millimetre ratio, the dimensions were readily found. The pitch of the threads was measured to be practically equal to 2.0 mm, which is the correct pitch for the current bolts according to ISO 4014 [16]. As seen in Figure 11, the major diameter of the bolt threads is 15.88 mm, and the minor diameter of the nut threads is 14.05 mm. These two diameters are both within the tolerances specified by ISO

965-1 [23] (tolerance classes 6g and 6H). Note that only three of the threads in the nut have a full height; see Figure 11b. The other threads have a reduced height. Alexander [1] noted that this so-called bell-mouth shape of the hole of the nut can affect the tensile strength of threaded assemblies because the bell-mouth influences the total shear area of the engaged threads.

Figure 12 displays the geometry, boundary conditions, and discretization of the axisymmetric FE model. The circular plates of the test grips were included to account for their elastic deformation and the friction between the bearing face of the nut and the corresponding plate. The steel plates were modelled as elastic materials. Note that the different heights of the nut threads were considered in the FE model, and the dimensions of these threads were based on the average values determined using the photo shown in Figure 11 and the pixel-to-millimetre ratio. The heights of the reduced and full-height nut threads were set to 1.82 and 2.31 mm, respectively.

The approximate element sizes in the model were 0.1 mm at the regions surrounding the engaged threads, 0.4 mm in the remaining part of the nut and threaded portion of the bolt, and 1.0 mm otherwise. The total number of elements was approximately 9000. Quadrilateral axisymmetric elements with reduced integration (CAX4R) were used for the entire model.

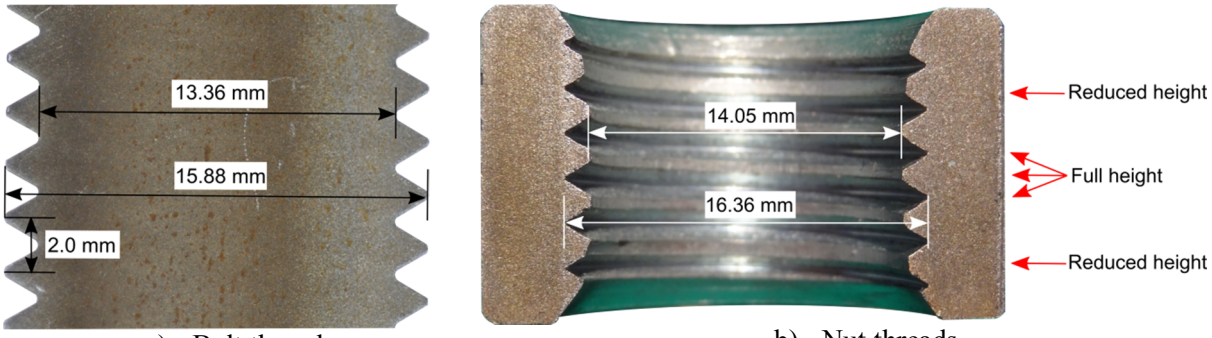

a) Bolt threads b) Nut threads

Figure 11 - Photos of the cross-sections used for the determination of thread sizes.

Post-print version of the paper by Grimsmo et al. in J Constr Steel Res, 126 (2016) 15-25
http://dx.doi.org/10.1016/j.jcsr.2016.06.023

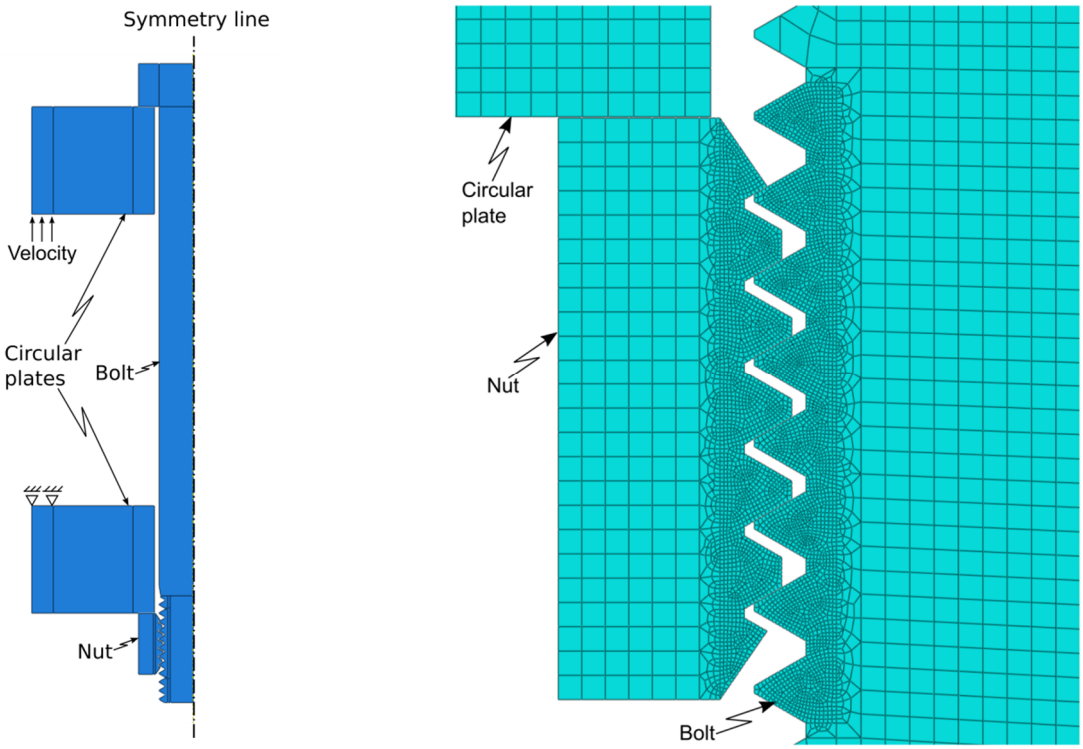

a) Entire model b) Thread engagement region

Figure 12 - Axisymmetric FE model (configuration: $L_g = 118$ mm and $L_t = 5$ mm).

5.2 Material model

An elastic-viscoplastic constitutive model implemented as a user subroutine (called VUMAT in Abaqus) was employed to describe the material behaviour. The model included linear elasticity, the von Mises yield criterion, the associated flow rule, non-linear isotropic hardening, and strain-rate hardening. The elastic behaviour was defined by the Young's modulus $E = 210$ GPa and Poisson's ratio $\nu = 0.3$. The equivalent stress σ_{eq} was described by:

$$\sigma_{eq} = \begin{cases} \sigma_y, & \varepsilon_p \leq \varepsilon_{p,plat} \\ \left[\sigma_y + \sum_{i=1}^{2} Q_i \left(1 - \exp\left(-\frac{\theta_i}{Q_i}(\varepsilon_p - \varepsilon_{p,plat})\right)\right)\right]\left[1 + \frac{\dot{\varepsilon}_p}{\dot{\varepsilon}_{ref}}\right]^C, & \varepsilon_p > \varepsilon_{p,plat} \end{cases} \quad (1)$$

where σ_y is the yield stress; Q_i and θ_i (where $i = \{1,2\}$) are the hardening constants of the extended Voce hardening rule; ε_p is the equivalent plastic strain; $\varepsilon_{p,plat}$ is the value of ε_p at the end of the yield plateau; $\dot{\varepsilon}_{ref}$ is the reference strain rate; and the C is a constant. The two latter parameters govern the strain-rate sensitivity. Viscous effects were included as plastic strain rates of more than

Post-print version of the paper by Grimsmo et al. in J Constr Steel Res, 126 (2016) 15-25
http://dx.doi.org/10.1016/j.jcsr.2016.06.023

0.1 s^{-1} occurred in the deforming threads, whereas the plastic strain rate in the core of the bolt was typically 10^{-4}-10^{-3} s^{-1}.

Failure was implemented by the extended Cockcroft-Latham criterion proposed by Gruben et al. [24]. The criterion states that failure occurs when the plastic work expressed with the integral

$$W = \int_0^{\varepsilon_p} \left\langle \phi \frac{\sigma_I}{\sigma_{eq}} + (1-\phi) \frac{(\sigma_I - \sigma_{III})}{\sigma_{eq}} \right\rangle^{\gamma} \sigma_{eq} d\varepsilon_p \tag{2}$$

attains a critical value W_{cr}. Here, $\langle \cdot \rangle$ are the Macaulay brackets, which ensures a nonnegative integrand; σ_I and σ_{III} are the first and third principal stresses of the Cauchy stress tensor; and ϕ and γ are material constants. As seen from Equation (2), W is essentially stress integrated over plastic strain, which means that the failure criterion is energy based. Moreover, the failure criterion takes into account strain-rate sensitivity through Equation (1), and it further depends on stress triaxility and Lode angle through the principal stresses. The reader is referred to Gruben et al. [24] for a more elaborate discussion on the failure criterion. Simulations with the original Cockcroft-Latham criterion, corresponding to the case with $\phi = \gamma = 1$, did not result in shear fracture of the threads; therefore, the extended criterion was employed.

The parameters identified for the PT bolt material are provided in Table 2. From the independent material tests performed on the specimen in Figure 4, true stress-strain curves were acquired. The yield stress σ_y and the plateau strain $\varepsilon_{p,plat}$ were read directly off from a representative stress-strain curve. Initial values for the hardening parameters Q_i and θ_i were obtained by fitting the expression in Equation (1) to the representative stress-strain curve from yielding to incipient necking. Subsequently, the material tension tests were simulated, and the hardening parameters were optimized to achieve a good agreement between the tests and simulation for the post-necking response as well, as shown in Figure 13.

Post-print version of the paper by Grimsmo et al. in J Constr Steel Res, 126 (2016) 15-25
http://dx.doi.org/10.1016/j.jcsr.2016.06.023

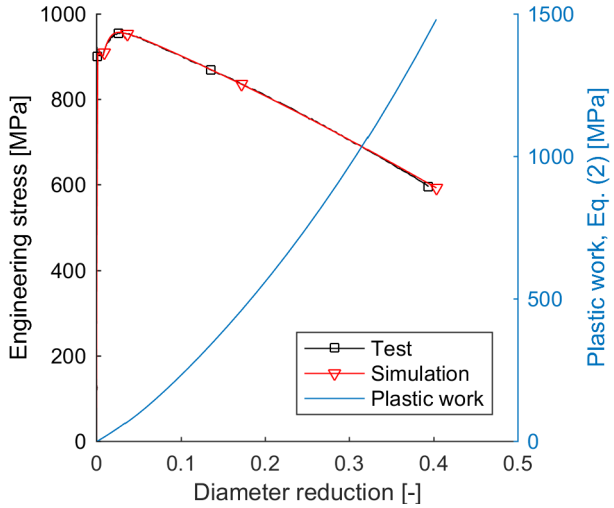

Figure 13 - Engineering stress versus diameter reduction at the neck obtained from a representative material tension test and a corresponding simulation, and the evolution of the plastic work W throughout the simulation.

The two fracture parameters, ϕ and γ, were set to 0.355 and 1.55, respectively. These values were calibrated for Docol 600DL steel by Gruben et al. [25], and gave reasonable results for the simulations presented herein. The fracture parameter W_{cr} was determined from the simulation of the material tension tests as follows. The stress and strain histories were acquired from the centre element at neck of the specimen, where fracture was expected to initiate. Subsequently, the integral in Equation (2) was calculated from zero deformation up to the deformation that corresponded to failure in the test, as illustrated in Figure 13. The final value of 1480 MPa then equalled the fracture parameter W_{cr}. As fracture parameters are in general relatively mesh dependent [26], it was investigated whether simulations with element size of 0.1 and 0.4 mm gave significantly different values for W_{cr}. A difference of only 2 % was obtained. Further, the response in component test simulations are mainly governed by plastic deformation rather than fracture. Therefore, one value for W_{cr} was used for the entire model shown in Figure 12.

Grimsmo et al. [27] determined the strain rate sensitivity parameters to be $\dot{\varepsilon}_{ref} = 10^{-3}$ s^{-1} and $C = 0.011$ for a bolt material of grade 8.8. These values were adopted for the current study. In Section 3.2, the yield strength of the nut was estimated to be 697 MPa. The nut material was therefore given this yield strength, whereas the remaining material parameters of the nut were assigned the values of the bolt material. The accuracy of these assumptions is evaluated in Section 5.5.

Post-print version of the paper by Grimsmo et al. in J Constr Steel Res, 126 (2016) 15-25
http://dx.doi.org/10.1016/j.jcsr.2016.06.023

Table 2 - Material parameters identified from material tension tests, hardness tests and inverse modelling.

	σ_y [MPa]	Q_1 [MPa]	θ_1 [MPa]	Q_2 [MPa]	θ_2 [MPa]	$\varepsilon_{p,plat}$ [-]	W_{cr} [MPa]
PT bolt	908.7	99.70	5194	3131	293.6	0.013	1480
Nut	697.4	99.70	5194	3131	293.6	0.013	1480

5.3 Boundary conditions and contact

Axisymmetric boundary conditions were applied to the entire model. A portion of the upper edge of the bottom circular plate was fixed in the vertical direction, as indicated in Figure 12a. The assembly was loaded by applying a constant velocity to a corresponding portion of the lower edge of the top circular plate. As the material was modelled as strain-rate dependent, the applied velocity was set approximately equal to that in the tests. The duration of each test was approximately 500 s; therefore, mass scaling with a factor of 10^7 was introduced to decrease the computational time in the simulations. The kinetic energy was found to be negligible compared with the strain energy.

Surface-to-surface contact was employed between the appropriate surface pairs, i.e., bolt head to circular plate, nut to circular plate, and nut threads to bolt threads. In addition, self-contact was applied to the surfaces of the engaged threads to prevent the threads from penetrating themselves. The chosen contact properties were “hard” contact in the normal direction and an isotropic Coulomb friction model in the tangential direction. The friction coefficient was set to 0.2. Friction influences the thread failure strength, as reduced friction allows the nut to dilate more freely [1]. The effect of varying the friction coefficient is not investigated herein.

5.4 Validation

The FE model was validated by comparing the numerical predictions with the results from the PT bolt tests with threaded lengths L_t equal to 9 and 17 mm. These lengths were chosen because they exclusively gave thread failure or bolt fracture, respectively. Of particular interest was whether the model could reproduce the experienced failure modes. Figure 14 provides three picture frames that show how thread failure developed during the simulation for the case of $L_t = 9$ mm, including fringe plots of the von Mises stress. The three frames in the figure show respectively the undeformed configuration, when yielding of the threads has initiated, and when thread failure has occurred. Diffuse necking of the threaded bolt shank caused an inward radial displacement of the engaged bolt threads. This effect reduced the overlap of these threads with the nut threads. In fact, pair ① of the initially engaged threads became disengaged, as observed from the bottom frame in

Post-print version of the paper by Grimsmo et al. in J Constr Steel Res, 126 (2016) 15-25
http://dx.doi.org/10.1016/j.jcsr.2016.06.023

Figure 14. The remaining engaged threads consequently experienced a greater loading, and the bolt threads eventually failed. From the test specimens that failed by thread failure, it was observed that some bolt threads were sheared off, whereas others were mostly bent; see Figure 10a. The bottom frame of Figure 14 demonstrates that this occurred because the bolt threads engaged with nut threads of reduced height were sheared off (see pair ② of the engaged threads), whereas a combination of shearing and bending occurred for the bolt threads engaged with nut threads of full height (see pair ③ of the engaged threads). Although not visible in Figure 14, some nut dilation was also observed by closely examining the simulation results. Note that the bolt also contracted radially prior to necking due to elongation in the longitudinal direction. However, this contraction obviously occurred for all threaded lengths and therefore did not dictate the failure mode.

Figure 15 provides the force-displacement curves obtained from the simulation and two corresponding tests. Recall that two out of the five replicate tests were recorded with a camera to allow for DIC analysis. The displacement in this plot and in the remaining plots of this paper is defined as the vertical displacement of the head of the bolt relative to the nut. Good agreement is observed in terms of the initial stiffness and the maximum force. In addition, the displacement at failure is reproduced in a satisfactory manner by the model. The minor oscillations observed for the simulation curves in Figure 15 stem from the mass scaling and can be neglected because they are only prominent at the start and the end of the simulation.

Post-print version of the paper by Grimsmo et al. in J Constr Steel Res, 126 (2016) 15-25
http://dx.doi.org/10.1016/j.jcsr.2016.06.023

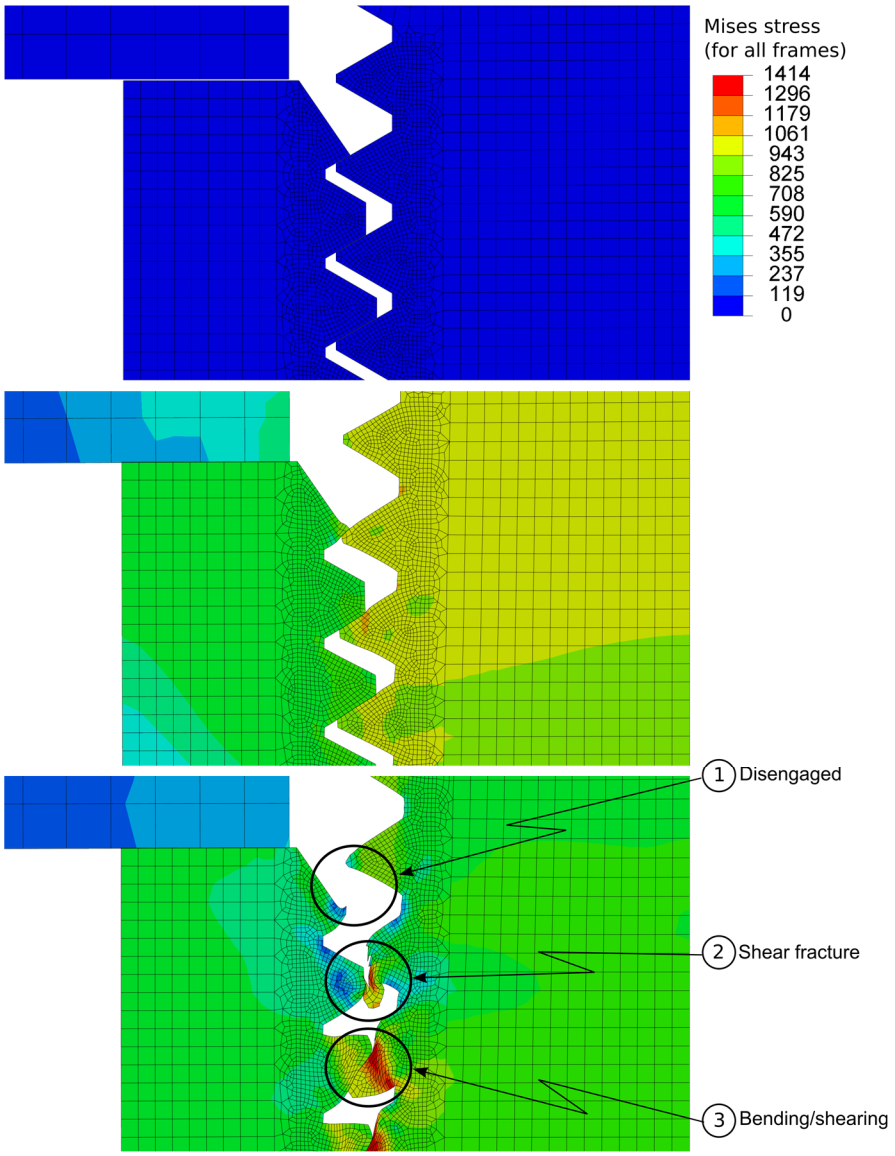

Figure 14 - Deformed threads at three stages: undeformed (top), initiation of yielding (centre), and thread failure (bottom). Obtained for $L_t = 9$ mm. The numbers attached to the bottom frame label the pairs of engaged threads.

Figure 16a displays how the specimen failed in a simulation where the threaded length $L_t = 17$ mm. Here, the increased threaded length L_t allowed necking to occur without appreciably influencing the thread overlap of the engaged threads. Thus, as observed in the corresponding tests, bolt fracture occurred. Considering the force-displacement curves in Figure 16b, there is an excellent agreement between tests and simulation up to 4 mm displacement. Beyond this displacement, the curves deviate and failure occurred at an approximately 18% larger displacement in the simulation compared with the tests. This could be due to the assumption of axisymmetry in

Post-print version of the paper by Grimsmo et al. in J Constr Steel Res, 126 (2016) 15-25
http://dx.doi.org/10.1016/j.jcsr.2016.06.023

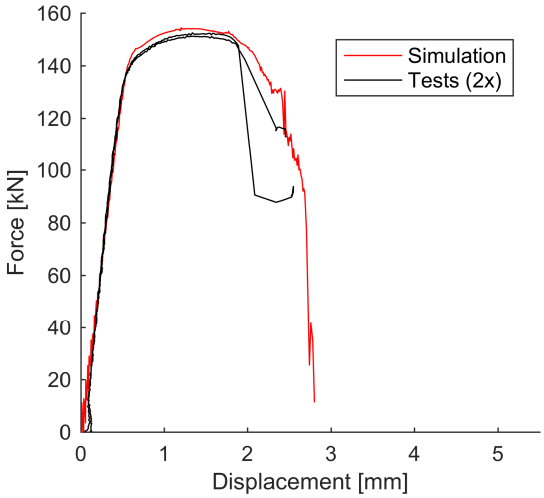

Figure 15 - Force vs. relative displacement of the bolt head to the nut obtained from two replicate tests and the corresponding simulation with $L_t = 9$ mm. Thread failure occurred in the tests and simulation.

the simulation because it did not allow for the slanted fracture surface shown in Figure 10b, which was experienced in most of the tests. Nevertheless, the model predicted failure adequately for the purposes of this study, and the correct failure mode was captured.

5.5 Varying yield strength and hardening of the nut

There are some uncertainties regarding the material properties of the nut because only hardness tests were performed on the nut material. It was therefore appropriate to investigate the sensitivity of the simulations with respect to some of the material parameters of the nut. The yield strength of the nut was estimated to be 697 MPa from the hardness measurements described in Section 3.2. This value is approximately 20% lower than the measured yield strength of the PT bolt material. To study the accuracy of this estimate, three additional simulations were conducted with nut yield strengths $\sigma_{y,nut}$ of 600, 800, and 900 MPa. For this parametric study, the case with threaded length $L_t = 9$ mm was chosen, which produced thread failure in all five replicate tests and the corresponding simulation; see Section 4.2 and 5.4. The results from the parametric study are shown in Figure 17a. Thread failure occurred in all simulations, but increasing the nut strength enhanced the displacement at failure. From these results, it seems that $\sigma_{y,nut} = 697$ MPa, which was estimated from the hardness measurements, provides a good prediction of the displacement at failure observed from the tests.

Post-print version of the paper by Grimsmo et al. in J Constr Steel Res, 126 (2016) 15-25
http://dx.doi.org/10.1016/j.jcsr.2016.06.023

a) Failure by bolt fracture

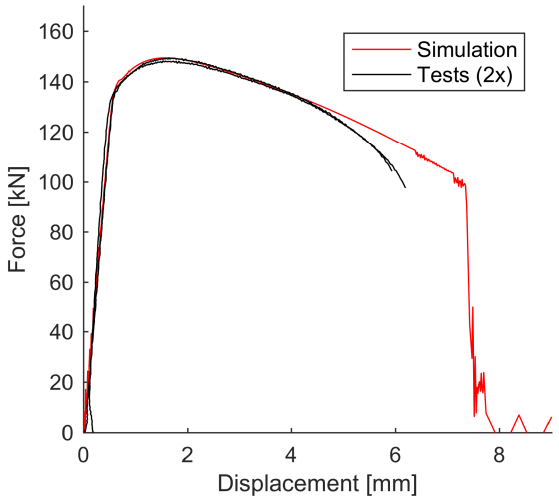

b) Force-displacement curves obtained from two replicate tests and the corresponding simulation

Figure 16 - Results with $L_t = 17$ mm. Bolt fracture occurred in the tests and simulation.

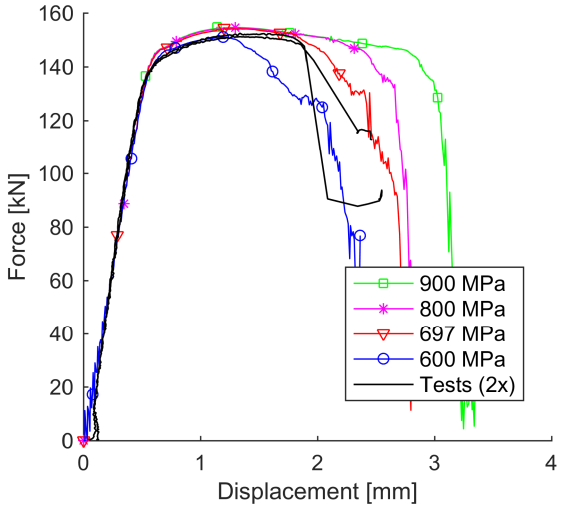

a) Varying yield strength $\sigma_{y,nut}$ (experimentally estimated: 697 MPa)

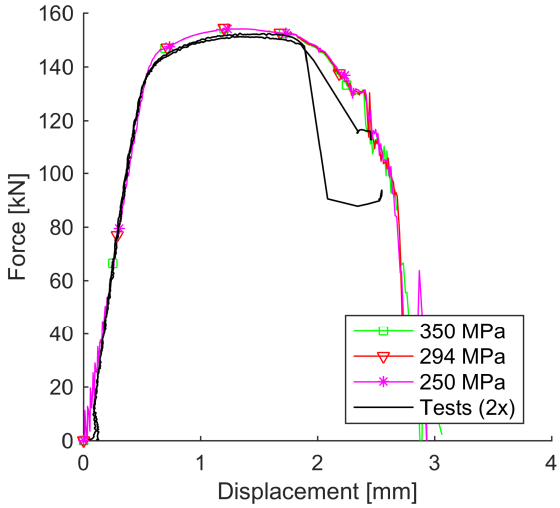

b) Varying hardening parameter θ_2 (experimentally estimated: 294 MPa)

Figure 17 - Effect of changing the yield strength and hardening of the nut ($L_t = 9$ mm).

Besides the yield strength, the nut was assigned the material parameters of the bolt given in Table 2, including the hardening parameters, Q_i and θ_i. It was chosen to investigate how the response was affected by varying the parameter θ_2, which mainly governs post-necking hardening of the materials. This parameter was determined in Section 3.1 to be 294 MPa. Figure 17b shows that the response is practically unaffected by varying θ_2 within the range of 250 MPa to 350 MPa. In these

simulations, the yield strength of the nut was set to the experimentally determined value of 697 MPa.

5.6 Simulation with a high nut

An alternative to the regular nut used in the tests and simulations presented previously is a high nut manufactured according to ISO 4033: *Hexagon high nut* [28]. For M16 nuts, the high nut is approximately 2 mm higher than the regular nut, which allows it to contain one more thread over the height. The other dimensions of the nut are identical to those of the regular nut. Figure 18 shows the simulation results with the two nut types and threaded length $L_t = 5$ mm, which is the shortest threaded length used in the tests. Thus, this was the configuration in the tests where thread failure was most prone to develop. As noted from Table 1, all experimental tests conducted with this threaded length failed by thread failure. As opposed to the simulation employing a regular nut, the simulation with a high nut predicted bolt fracture, as seen in Figure 18a. It is clearly visible how necking affected the effective overlap of the engaged threads. As indicated in the figure, the first and second initially engaged threads became disengaged in the simulation. Thread failure was prevented by the additional thread of the high nut. The force-displacement curves in Figure 18b display how the high nut caused an increase of approximately 400% in the displacement at failure. Note that the maximum force predicted by the regular and high nut simulations was approximately 5% greater than in the test. The plastic deformation occurred over a relatively short threaded length L_t of only 5 mm, where the thread run-out of the bolt shank was a significant portion of this length (approx. 1-2 mm). Thus, the difference in the maximum force may be explained by the axisymmetric model failing to capture the actual geometry of the thread run-out.

Post-print version of the paper by Grimsmo et al. in J Constr Steel Res, 126 (2016) 15-25
http://dx.doi.org/10.1016/j.jcsr.2016.06.023

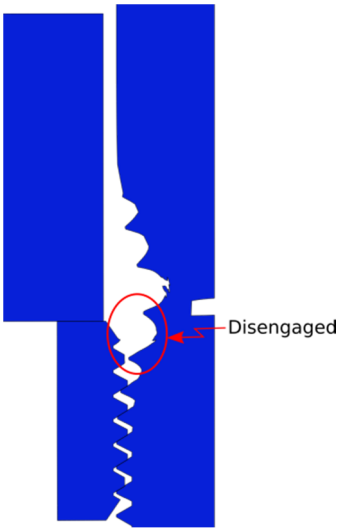

a) Failure by bolt fracture obtained with a high nut

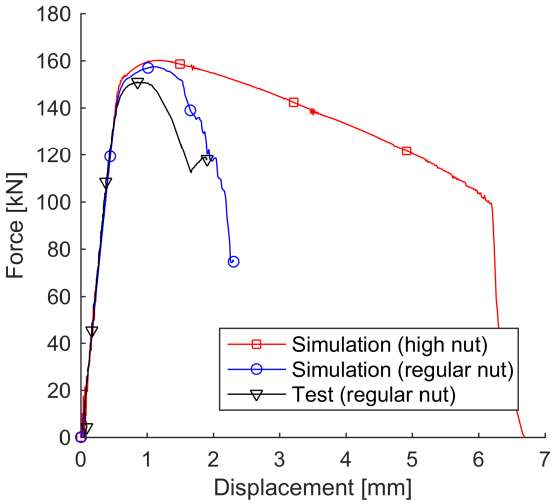

b) Force-displacement curves. Simulation and test with regular nut is included for comparison

Figure 18 - Results obtained from simulations performed with a high nut ($L_t = 5$ mm).

6 Discussion

An axisymmetric FE model does not capture the helical shape of the threads. Chen and Shih [29] demonstrated that an axisymmetrical model with an elastic material gave a slightly different load distribution at the threads than that of a three-dimensional model. Nevertheless, the results from the simulations in this paper demonstrate that an axisymmetric model provided adequate results for the purposes of this study.

The bolts tested herein were only loaded under tension. In many cases, bolts can also be subjected to shear forces and/or eccentric axial forces, which may impose a non-symmetric pressure distribution onto the bearing face of the nut. This may further increase the likelihood of thread failure.

The probability of thread failure can be reduced by an appropriate selection of fasteners. The code NS-EN 1090-2: *Execution of steel structures and aluminium structures – Part 2* [30] requires at least one full thread (in addition to the thread run-out) in the grip for non-preloaded bolts, whereas four full threads in the grip are required for preloaded bolts. The purpose of these requirements is to ensure correct installation without jamming the nut on the thread run-out of the bolt. For the bolts tested here, it appears that these requirements are inadequate if bolt fracture is the desired failure mode. To determine whether this observation is generally representative, more tests on bolts

of different dimensions, steel grades, and standards are necessary. Nevertheless, if thread failure is undesired, it may be good practice to choose fully threaded bolts when the bolts are primarily tension loaded. This applies to both the case of external loading and pre-loading. Alternatively, the possibility of thread failure can be reduced by the introductions of washers and shims because these increase the threaded length L_t. If it is not feasible to avoid few threads in the grip, then either high nuts or two regular nuts could be employed.

7 Concluding remarks

Direct tension tests have been performed on partially and fully threaded bolt and nut assemblies. It was examined how the length L_t of threaded bolt shank within the grip determined the failure mode. Thread failure occurred in the tests conducted with short lengths L_t, whereas bolt fracture took place for sufficiently long L_t. Both failure modes were observed for intermediate L_t. For the tests with short L_t, a slight increase in the maximum force was experienced, and diffuse necking of the bolt shank occurred close to the nut. Both these effects likely contributed to thread failure, which produced failure at a comparatively low deformation level. FE simulations revealed that necking reduced the overlap of the engaged threads, and some of these threads were eventually disengaged during the simulations. Subsequently, the remaining engaged threads failed by a combination of bending and shearing. The simulations demonstrated that changing the nut strength did not prevent thread failure, whereas the introduction of a high nut with one additional thread inhibited this failure mode.

In conclusion, the probability of thread failure can be reduced by increasing the length L_t or by increasing the nut height, i.e., the thread engagement length. Thus, for bolts subjected to tension, either by external loading or pre-loading, it may be advantageous to use fully threaded rather than partially threaded bolts. Alternatively, washers, shims, high nuts or two nuts together can be used to reduce the probability of thread failure.

Acknowledgements

The work has received financial support from the Research Council of Norway through the SFI scheme. We would like to thank Prof. Emeritus P. K. Larsen for feedback on the work. We would also like express our gratitude towards MSc. T. Auestad, MSc. E. Skavhaug, and MSc. S. Østhus for assisting us with the experimental tests.

References

[1] E.M. Alexander, Analysis and design of threaded assemblies. Paper No. 770420, SAE Transactions, 1977.
[2] International Organization for Standardization (ISO), ISO 898-2, mechanical properties of fasteners made of carbon steel and alloy steel - Part 2: nuts with specified property classes - coarse and fine pitch thread, ISO, Switzerland, 2012.
[3] J.A. Swanson, Characterization of the strength, stiffness and ductility behavior of T-stub connections, PhD dissertation, Georgia Institute of Technology, Atlanta, GA, 1999.
[4] J.H. Bickford, S. Nassar, Handbook of Bolts and Bolted Joints, CRC Press, New York, NY, 1998.
[5] B. Bose, Z.M. Wang, S. Sarkar, Finite-element analysis of unstiffened flush end-plate bolted joints, J Struct Eng-ASCE, 123 (1997) 1614-1621.
[6] W. Grogan, J.O. Surtees, Experimental behaviour of end plate connections reinforced with bolted backing angles, J Constr Steel Res, 50 (1999) 71-96.
[7] A.M. Girão Coelho, F.S.K. Bijlaard, L. Simões da Silva, Experimental assessment of the ductility of extended end plate connections, Eng Struct, 26 (2004) 1185-1206.
[8] B. Yang, K.H. Tan, Experimental tests of different types of bolted steel beam-column joints under a central-column-removal scenario, Eng Struct, 54 (2013) 112-130.
[9] R.A. Herrera, M. Bravo, G. Gómez, G. Aedo, Performance of built-up T-stubs for Double T moment connections, J Constr Steel Res, 88 (2013) 289-295.
[10] E.L. Grimsmo, A.H. Clausen, M. Langseth, A. Aalberg, An experimental study of static and dynamic behaviour of bolted end-plate joints of steel, Int J Impact Eng, 85 (2015) 132-145.
[11] E.W.J. Troup, E. Chesson Jr., Calibration Tests of A490 High-Strength Bolts, in: Civil Engineering Studies SRS-280, University of Illinois Engineering Experiment Station, College of Engineering, University of Illinois at Urbana-Champaign, Champaign, IL, 1964.
[12] G.H. Sterling, J.W. Fisher, Tests of A490 bolts, preliminary report, Mardi 1964, Fritz Laboratory Reports, 1964.
[13] H. Fransplass, M. Langseth, O.S. Hopperstad, Tensile behaviour of threaded steel fasteners at elevated rates of strain, Int J Mech Sci, 53 (2011) 946-957.
[14] H. Fransplass, M. Langseth, O.S. Hopperstad, Numerical study of the tensile behaviour of threaded steel fasteners at elevated rates of strain, Int J Impact Eng, 54 (2013) 19-30.
[15] J.J. Amrine, J.A. Swanson, Effects of variable pretension on the behavior of bolted connections with prying, Eng J, 41 (2004) 107-116.
[16] International Organization for Standardization (ISO), ISO 4014, hexagon head bolts - product grades A and B, ISO, Switzerland, 2011.

[17] International Organization for Standardization (ISO), ISO 4017, hexagon head screws - Product grades A and B, ISO, Switzerland, 2014.
[18] International Organization for Standardization (ISO), ISO 4032, hexagon regular nuts (style 1) - product grades A and B, ISO, Switzerland, 2012.
[19] European Committee for Standardization (CEN), NS-EN 15048-1, Non-preloaded structural bolting assemblies - Part 1: general requirements, Norwegian Standard, 2007.
[20] European Committee for Standardization (CEN), NS-EN 14399-1, high-strength structural bolting assemblies for preloading - Part 1: general requirements, Norwegian Standard, 2015.
[21] International Organization for Standardization (ISO), ISO 898-1, mechanical properties of fasteners made of carbon steel and alloy steel - Part 1: nuts with specified property classes - coarse and fine pitch thread, ISO, Switzerland, 2013.
[22] Dassault Systémes, Abaqus 6.14 documentation, Simulia Systems, Providence, RI, 2014.
[23] International Organization for Standardization (ISO), ISO 965-1, ISO general purpose metric screw threads - Tolerances, ISO, Switzerland, 2013.
[24] G. Gruben, O.S. Hopperstad, T. Borvik, Evaluation of uncoupled ductile fracture criteria for the dual-phase steel Docol 600DL, Int J Mech Sci, 62 (2012) 133-146.
[25] G. Gruben, O.S. Hopperstad, T. Børvik, Simulation of ductile crack propagation in dual-phase steel, Int J Fracture, 180 (2013) 1-22.
[26] S. Ehlers, J. Broekhuijsen, H.S. Alsos, F. Biehl, K. Tabri, Simulating the collision response of ship side structures: A failure criteria benchmark study, Int Shipbuilding Progress, 55 (2008) 127-144.
[27] E.L. Grimsmo, A.H. Clausen, A. Aalberg, M. Langseth, A numerical study of beam-to-column joints subjected to impact, Eng Struct, 120 (2016) 103-115.
[28] International Organization for Standardization (ISO), ISO 4033, hexagon high nuts (style 2) - product grades A and B, ISO, Switzerland, 2012.
[29] J.J. Chen, Y.S. Shih, Study of the helical effect on the thread connection by three dimensional finite element analysis, Nucl Eng Des, 191 (1999) 109-116.
[30] European Committee for Standardization (CEN), NS-EN 1090-2: Execution of steel structures and aluminium structures - Part 2: Technical requirements for steel structures, Norwegian Standard, 2008.